Journal Name

ARTICLE TYPE

Cite this: DOI: 00.0000/xxxxxxxxxx

# Reduction of $O_2$ to $H_2O_2$ using Small Polycyclic Molecules[†]

Kristal Lopez,[a] and Michael N Groves*[a]

Received Date
Accepted Date

DOI: 00.0000/xxxxxxxxxx

Hydrogen peroxide is an environmentally friendly oxidizing agent that is important in several industries. It is currently produced industrially via the anthrahydroquinone (AHQ) process where $O_2$ reacts with a functionalised version of anthrahydroquinone to produce $H_2O_2$ and anthraquinone. In the previously published DFT pathway for this process the transition of the $OOH^{\cdot}$ radical across the partially dehydrogenated AHQ catalyst was not explored. In this paper, we will use DFT to explore this step and show that there is a deep potential energy minimum that inhibits the $OOH^{\cdot}$ from being fully reduced. We then examine other similar sized polycyclic molecules with two OH-groups on the same side that could serve as alternative catalysts without this issue. In this analysis, we identify phenanthraquinone as a possible alternative and present the pathway for this candidate to produce $H_2O_2$ as well as its regeneration with $H_2$.

## 1 Introduction

Hydrogen peroxide ($H_2O_2$) is used in many industries including as a bleaching agent for paper production[1–5] and water treatment[6–8]. Worldwide production exceeds 5.5 million metric tons in 2015 and it continues to climb[3]. It is also used in several other applications including the synthesis of organic chemicals such as Propylene Oxide through the hydrogen peroxide propylene oxide (HPPO) process where hydrogen peroxide is used as the oxidant[9,10]. HPPO is the integration of two processes: first the anthraquinone (AQ) process synthesizes hydrogen peroxide and is then integrated with the propene epoxidation process catalyzed by titanium silicalite[11]. Hydrogen peroxide can also serve as an alternative energy carrier in fuel cell applications. Fuel cells traditionally use oxygen as the oxidant, but in a recent investigation $H_2O_2$ was used not only as an alternative oxidant but as a reductant making the cell structure simpler[12]. Theoretically, it would provide a higher power output compared to fuel-cells where oxygen is the oxidant.

There are multiple ways under study to synthesize $H_2O_2$. The $2e^-$ electrochemical processes has recently been gaining in popularity. The focus has been on a water electrolyzer configuration instead of a hydrogen-based fuel cell type system due to the high cost and storage of $H_2$ gas[13]. In this system, metallic[14–17] and non-metallic[18–22] electrode materials have been studied. A second method to synthesize $H_2O_2$ is direct synthesis from $H_2/O_2$ mixtures in a high-pressure gas like $CO_2$ or $N_2$. In these cases, a Pd-based catalyst is used and the high-pressure gas is meant to limit the fire hazard given the explosive nature of $H_2/O_2$ mixtures as well as the inclusion of methanol as a solvent[13]. Supercritical $CO_2$ has also been explored as a solvent to replace methanol, however, the reaction temperature plays a significant role. In a study by Landon *et al*. they observed that the critical temperature of $CO_2$ was high enough to promote a high decomposition rate of $H_2O_2$. They found that temperatures around 274 K with Pd-Au catalysts and methanol as the solvent results in high yields of $H_2O_2$[23]. A third method to synthesize hydrogen peroxide is via the gas-phase reaction of a $H_2/O_2$ non-equilibrium plasma[24,25]. This method has the benefit of not needing any catalysts or added chemicals, however, it does not draw much attention over safety concerns. A double dielectric barrier discharge reactor can safely work with 30 mol% $O_2$ content[26] which is much higher than the typical 6% explosion limit[27]. A fourth method involves the UV illumination of an aqueous suspension of $TiO_2$ particles. The efficiency of this photochemical process can be significantly improved with the addition of $Cu^{2+}$[28]. However, the most common way to synthesize $H_2O_2$ is via the AQ process[29], which is illustrated in Figure 1. In industry, the majority of $H_2O_2$ is produced using the AQ process. It consists of two processes: the hydrogenation process and the autoxidation process[29]. $H_2O_2$ is synthesized in the autoxidation step and the catalyst is regenerated with $H_2$ on a Pd catalyst to form anthrahydroquinone (AHQ). This process is energy intensive and damages the environment so until a scalable alternative exists it is important to examine and improve the current process to minimize these effects.

In this project, the focus is on the autoxidation step in the AQ process. In the autoxidation step, the triplet $O_2$ and AHQ produce singlet $H_2O_2$ and AQ under ambient conditions. In a previous study, density functional theory was used to examine the the autoxidation step of the AQ process[2]. In this work a crucial

---

[a] *California State University, Fullerton, Fullerton, CA, 92831, USA. Fax: +1(657)278-5316; Tel: +1(657)278-7018; E-mail: mgroves@fullerton.edu*

[†] Electronic Supplementary Information (ESI) available: [details of any supplementary information available should be included here]. See DOI: 00.0000/00000000.

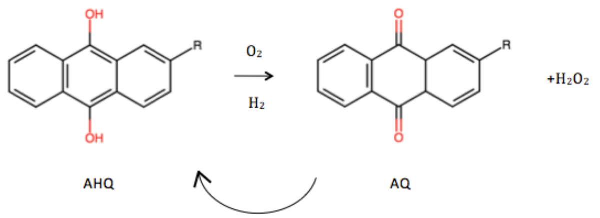

Fig. 1 The overall anthraquinone process. The second half of the reaction is known as the autoxidation step.

step is missing where the hydroperoxyl (OOH˙) radical transitions across the partially dehydrogenated AHQ molecule to perform the second hydrogen abstraction. Given that the overall AQ process is still being determined[30,31], the goal of this investigation is to calculate the transition of the OOH˙ across the AHQ molecule in an effort to examine one of many possibilities so that an accurate representation of this process can be determined. It was found that this transition has a deep potential well in the singlet state that probably acts as the rate-determining step as the OOH˙ transitions across the AHQ molecule. Alternative catalysts will be explored with both OH-groups on the same side of the molecule, which eliminates the need for the intermediate to move across the catalyst. Phenanthraquinone has been identified as an alternative catalyst, and the barriers of the autoxidation and hydrogenation steps will be presented and compared to those from AHQ to reduce $O_2$ to $H_2O_2$.

## 2 Methods

All calculations are performed using the Python-based density functional theory (DFT) software GPAW[32,33] supported by the Atomic Simulation Environment (ASE)[34]. The generalized gradient approximation (GGA) using the Perdew, Burke, and Ernzerhof (PBE)[35] exchange-correlation functional was used. Dispersion interactions were taken into account using the Tkatchenko-Scheffler method[36]. All reported results use a Monkhorst-Pack $\vec{k}$-point mesh of $2 \times 2 \times 1$, and a grid spacing below 0.1775 based on a convergence test presented in Table S1. Molecular geometries are relaxed to a maximum force less than 0.02 eV/Å. In this project, the $O_2$ system has a triplet spin, and the $H_2O_2$ has a singlet spin; therefore, reaction pathways with both spins are calculated. This accomplished by performing spin polarized calculations where the magnetic moment is fixed to 2.0 for triplet state calculations, and 0.0 for the singlet state calculations.

Reaction barriers are calculated between intermediates to find the transition states. The nudged elastic band (NEB) method is used to find minimum energy paths (MEP)[37]. The automated nudged elastic band (AutoNEB) algorithm is an add-on to the basic NEB method that effectively locates transition states because it focuses resources to better characterize less resolved regions along the MEP[38]. The AutoNEB runs with the same basic NEB algorithm, where it will initialize a pathway with a user designated number of images, however, it then iteratively adds and relaxes more images until a predetermined total number of images is achieved. This converges a rough pathway and once the region around the saddle point is resolved, a climbing image is used to converge the transition state[38].

## 3 Results and discussion

The calculated reaction pathway for reducing $O_2$ to $H_2O_2$ is shown in Figure 2. All reported energies for Figure 2 use the separated $O_2$/AHQ triplet state as the reference. The triplet reaction pathway (purple line) begins with the formation of a hydrogen bond between the $^3O_2$ and the AHQ molecule resulting in an energy of -0.11 eV. The first hydrogen abstraction to the leading oxygen has a transition state energy of 0.174 eV. At some point the total spin must decrease since there is an energetic penalty to form $H_2O_2$ in the triplet state while it is energetically favorable to form $H_2O_2$ in the singlet state. Upon completion of the first hydrogen abstraction is when we predict the total spin to reduce to zero. This is based on how after the first hydrogen abstraction, the singlet and triplet state share similar energies (triplet: 0.144 eV; singlet: 0.151 eV) and they share similar positions. This does not occur again during the mechanism. From here, now in the singlet state (gold line), the OOH˙ rotates around the hydrogen bond formed between it and the partially dehydrogenated AHQ molecule (pAHQ) to present the other O atom towards the other OH-group on the pAHQ molecule. This is a barrierless transition that raises the energy of the system to 0.204 eV. This rotated state is what is illustrated in Figure 2. Then the OOH˙ transitions across the molecule and forms a bond with the carbon adjacent to the other OH-group. The energy of the transition state is 0.53 eV and the resulting intermediate has an energy of -0.795 eV. The energy of the transition state to break this carbon-oxygen bond and abstract the second hydrogen is at 0.16 eV and the energy of the resulting $H_2O_2$ molecule hydrogen bonded to the dehydrogenated AHQ molecule is -1.068 eV.

The identified location, just after the first hydrogen abstraction, is the most likely location for the total spin to reduce from 1 to 0 as there is a convergence in geometry and energy of the two states. Figure S1 in the supplemental information shows an expanded figure where four reaction pathways are illustrated: the two shown in Figure 2, the triplet pathway with the trailing oxygen in the OOH· hydrogenated, and the singlet pathway with the front oxygen in the OOH· hydrogenated. After the identified location where the total spin can relax from 1 to 0 the four pathways diverge in terms of energy and position. Thus it is unlikely that the transition between triplet and singlet states occurs at any other part of the reaction since it would probably involve some sort of electromagnetic emission which has not been previously reported.

Two dashed lines are included in Figure 2 and represent the separated OOH˙ molecule from the partially dehydrogenated

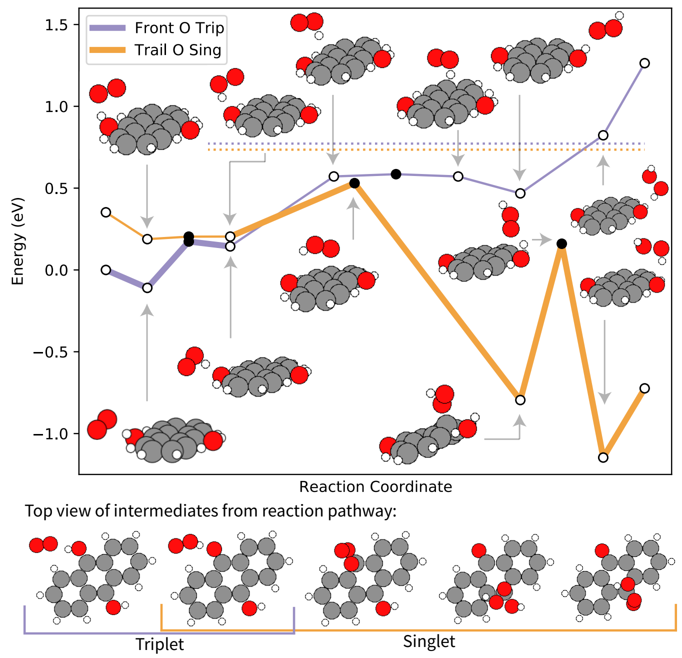

Fig. 2 The most favorable AHQ reaction pathway (outlined with bold lines) calculated for the reduction of $O_2$ to $H_2O_2$. Triplet spin calculations are in gold while singlet spin calculations are in purple. The path starts in the triplet state and the first hydrogen atom is abstracted to form $OOH^{\cdot}$. Then the $OOH\cdot$ reduces its total spin to 0 given that the triplet and singlet states are the same energy in this configuration. Then the $OOH^{\cdot}$ spins to present the unhydrogenated O atom and transitions across the AHQ to eventually become $H_2O_2$. Intermediates are indicated by the white dots, while transition states are indicated by black dots.

AHQ. Based on these calculations, the reduction of $O_2$ to $H_2O_2$ should stay on the same AHQ molecule as it is not energetically favourable for the $OOH^{\cdot}$ radical to separate from the catalyst. This result is inconsistent with a previous description of the AHQ process[28] where they state that this process follows a free-radical chain mechanism[39] that involves two separate AHQ molecules to form $H_2O_2$. However, in this description the starting catalyst has additional hydrogenation at the 9, and 10 position on the ring. In a more recent description of the industrial process[29] it is reported that additional hydrogenation tends to occur at the 5, 6, 7, and 8 position to a much greater degree and results in a less active catalyst than if the anthracene moiety was unsaturated. Given that the calculations included in this work more closely resemble the more recent description of the industrial process, we will conclude that the process involves only one AHQ molecule.

The results reported here are consistent with with the previously reported pathway by Nishimi *et al.*[2] when the difference in the reference state is taken into account. This includes considering a pathway where the $OOH^{\cdot}$ by-passes the deep potential energy minimum and forms a hydrogen bond with the second OH-group. In our calculations, no hydrogen bond could be formed and the hydrogen abstraction was always a barrierless process. This indicates that if the $OOH^{\cdot}$ species were to avoid the newly reported minimum that it should be facile for it to abstract the second hydrogen. In their calculations, Nishimi *et al.* also reported no barrier for this process. One notable exception is that in this work we were unable to calculate an intermediate where $OOH^{\cdot}$ formed a hydrogen bond with the remaining OH-group in the singlet state. Every attempt resulted in either no association with the OH-group or the formation of $H_2O_2$. In our case, stable $OOH^{\cdot}$ states were calculated above the partially dehydrogenated AHQ molecule halfway between the C=O and C−OH groups had the same energy as their reported case for the $OOH^{\cdot}$ hydrogen-bonded to the second OH-group.

The major difference between this work and what was presented by Nishimi *et al.* is that along the most favorable pathway presented in Figure 2 is a deep potential well where the $OOH^{\cdot}$ absorbs on to the carbon atom adjacent to the second OH-group. Nishimi *et al.* reported no information on the transition along the AHQ molecule after the first hydrogen abstraction[2]. This calculated pathway serves as an extension to their work and demonstrates that there is a location where the reaction falls into a significant potential energy well. The appearance of this major binding site for the $OOH^{\cdot}$ radical is explained by the same work of Nishimi *et al.* where they identify a molecular orbital at the location of that carbon atom after the first hydrogen abstraction that could adsorb the radical as it transitions across the surface.

In general, the $H_2O_2$ synthesis mechanism is typically described as a radical chain sequence, and there are many side products which may be produced and consumed in the overall process. For example, the frequently cited representation of the synthesis of $H_2O_2$ using 9,10-dihydroxy-9,10-dihydroanthracene published by Campos-Martin et al. illustrate one proposed mechanism with many side products[28]. In a recent paper, Korth and Mulder[31] argues that the previously calculated activation barrier for the first hydrogen abstraction by Nishimi *et al.*[2], which is proposed to be the rate determining step is too small. Korth and Mulder estimate that the rate of the reaction based on the Nishimi *et al.* barrier is $1.4 \times 10^6$ $M^{-1}$ $s^{-1}$. Korth and Mulder argue that the speed at which that reaction proceeds would make the rate of dissolution of $O_2$ into the solvent the rate-limiting process. Since $O_2$ dissolution has not been reported in the literature as the rate-limiting process implies that the rate determining step must have a larger barrier. In its place, based on many other hydrogen abstraction processes by $^3O_2$ and $HO_2\cdot$ from arenols, aryloxyls and their tautomers, they suggest that oxanthrone, a tautomer of AHQ, plays a significant role in the synthesis of $H_2O_2$. Oxanthrone has a similar structure as the stable intermediate that is reported in our paper, however, our calculated pathway does not involve a tautomerization reaction. Instead, our proposed $H_2O_2$ peroxide synthesis reaction produces a similar type of structure to oxanthrone as a part of the mechanism instead of relying on hydrogen atoms transferring across the AHQ molecule. The 0.272 eV difference between our suggested intermediate and the formation of $H_2O_2$ provides enough of a thermodynamic driving force to complete the reaction. Additionally, the 0.955 eV activation energy between the intermediate and $H_2O_2$ formation also eliminates the concern that the first hydrogen abstraction step is too shallow to account for the dissolution of $O_2$ being the rate determining step. Finally, similar adducts have also been calculated by Valgimigli *et al.*[40] for hydrogen abstraction by $O_2$ from 1,4-semiquinone.

Given the potential for the $OOH^{\cdot}$ radical in the favorable singlet state to be trapped in a deep potential well during the reaction, a search was performed to determine alternative small carbon-based catalysts that eliminate the need for a potential transit across the catalyst. Twelve alternatives were tested where the two OH-groups, or one OH-group and an acidic C−H (as is the case for benzo[a]fluorene) located on the same side of the each molecule. These twelve molecules were selected as all of them can exist with hydrogenated and dehydrogenated OH-groups like AHQ and AQ. The results of triplet and singlet state calculations for the hydrogenated catalyst with a separated $O_2$ molecule and the dehydrogenated catalyst with a separated $H_2O_2$ molecule are presented in Figure 3. Both spin states for both physical states are presented for reference.

Based on this search only two molecules present themselves as potential alternatives based on the energy of the singlet state calculation of the dehydrogenated catalyst with a separated $H_2O_2$ molecule relative to the triplet state calculation of the hydrogenated molecule with a separated $O_2$ molecule: phenanthraquinone and benzo[c]phenantherene. benzo[c]phenantherene is the only molecule which resulted in an exothermic energy difference. However, when benzo[c]phenantherene is dehydrogenated one of the oxygen atoms interacts with an adjacent carbon atom to close the ring. It is assumed that this ring closure will not be facile to reopen to regenerate the catalyst so it is disregarded. The other candidate, phenantrhaquinone, is essentially energetically equivalent for both the separated reactant case and separated product case. However, a similar motif has recently been credited for high electrochemical activity of graphene edges for $H_2O_2$ synthesis[41].

A full reaction pathway was calculated for the singlet and triplet pathways for the conversion of $^3O_2$ to $H_2O_2$ with phenanthraquinone. This is illustrated in Figure 4. As before, the system begins in the triplet state and is indicated by the purple line in the figure. All the following energies are relative to the separated $^3O_2$ and phenanthraquinone molecules in the triplet state. The reaction starts by $^3O_2$ forming a hydrogen bond with an OH-group over top of the phenanthraquinone molecule with an energy of -0.122 eV. The energy of the transition state to abstract the first hydrogen atom is 0.254 eV and the energy of the resulting $OOH^{\cdot}$ radical is 0.145 eV. As the first hydrogen is abstracted the $O_2$ translates to in front of the phenanthraquinone molecule. In the singlet state reaction pathway, however, the $OOH^{\cdot}$ molecule remains above the phenanthraquinone molecule. The shift in position of the $OOH^{\cdot}$ moiety in the triplet state means that there is no early location for the total spin to drop from 1 to 0, like in the AHQ case, as there is no overlap of both energy of the system and the positions of the molecules until much later in the reaction. This includes the transition states for both the singlet and triplet pathway for the first hydrogen abstraction: while they both have similar energies, the molecules are in different places. Moving forward along the reaction pathway, as the $OOH^{\cdot}$ begins the second hydrogen abstraction, the energy of the triplet and singlet states converge. The blue point on the plot at 0.622 eV illustrates where both the energy and position of both states overlap. From here the total spin of the system can drop to 0 and relax to form $H_2O_2$ in the singlet state which has an energy of -0.326 eV.

Based on the above reaction pathway, the formation of $H_2O_2$ is exothermic. Relative to the separated $O_2$ molecule in the triplet state, the total energy of the system drops to -0.326 eV for the adsorbed $H_2O_2$ molecule in the singlet state. This is important since this process is driven thermodynamically towards the $H_2O_2$ production. Furthermore, placing both OH-groups on the same side of the molecule seems to have the intended result where there is no deep intermediate that can kinetically inhibit the reaction. Extraction of the $H_2O_2$ might be a little challenging given that the energy of the separated $H_2O_2$ from the phenanthraquinone molecule is 0.013 eV higher than the separated $^3O_2$/phenanthrenehydroquinone. At 298.15 K and 1 atm, the $\Delta_r G$ calculated using the ideal gas limit for the separated reactants to the separated products is 0.078 eV. This results in an equilibrium constant, K, of 0.048. However, the minimum energy state along the reaction pathway is $H_2O_2$ adsorbed on phenanthraquinone. Therefore, the system would spontaneously form this state and produce $H_2O_2$. Once that occurs, the reaction conditions could change such that the barrier of the reverse reaction would inhibit $O_2$ formation so that the $H_2O_2$ could be extracted.

One interesting result from the above calculated pathway is that $H_2O_2$ would decompose into $^1O_2$. The lowest energy gold (singlet) pathway does not have a point where the energy and position of both molecules in the system overlap with the triplet state pathway. This means that the most favourable reverse reaction would result in singlet $O_2$ being produced. This result has been observed with carbocatalysts in the literature. The chemiluminescence phenomenon of luminol can be performed with $H_2O_2$. The accepted pathway involves the decomposition of $H_2O_2$ into $OH^{\cdot}$ and $O_2^{\cdot -}$ radicals resulting in chemiluminescence. Wang *et al.* reported that when this process was catalyzed using graphene oxide[42], and carbon nanodots[43] the $H_2O_2$ was decomposed into $^1O_2$ which lead to chemiluminescence. Wu and Han also report the production of $^1O_2$ from $H_2O_2$ with hollow fluorescent carbon nanoparticles[44]. All of these reports state that this decomposition follows a route that involves the formation of $OH^{\cdot}$ and $O_2^{\cdot -}$ radicals instead of $OOH^{\cdot}$ radicals, however, the formation of $^1O_2$ from an oxygenated carbocatalyst provides some support for this calculated pathway.

The hydrogenation step of the AQ catalyst is the most important step in the AQ process[29]. Due to its importance the barrier for the regeneration of dehydrogenated phenanthraquinone was performed. The barrier is 1.293 eV and is illustrated in Figure 5. The pathway begins with the $H_2$ molecule in front of the two oxygen atoms on phenanthraquinone. As the the hydrogen molecule approaches, it separates and the combined system relaxes in to the final form. A second pathway was tested where the $H_2$ molecule started above the molecule and resulted in an equivalent reaction pathway.

The regeneration of AQ in industrial settings uses a Pd catalyst[29]. This is because the two sites that need to be hydrogenated are distant enough that a catalyst surface is necessary to transport the two hydrogen atoms from $H_2$ to both sides. A DFT study by Kamachi *et al.* for the rehydrogenation of AQ on Pd(111) surface reported that the barriers for this two-step process are 0.6 eV and 0.7 eV for the first and second hydrogen abstractions respec-

| | 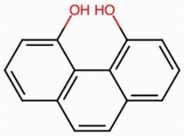 | 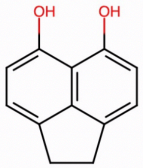 | 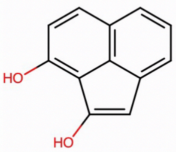 | 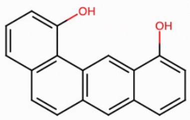 | 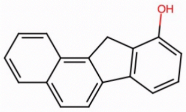 | 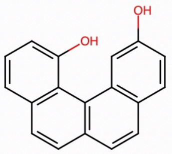 |
|---|---|---|---|---|---|---|
| | **Phenanthrene** | **Acenaphthylene (Top)** | **Acenaphthylene (Side)** | **Benz[a]anthracene** | **Benzo[a]fluorene** | **Benzo[c]phenanthrene** |
| Triplet $O_2$ (eV) | 0 | 0 | 0 | 0 | 0 | 0 |
| Singlet $O_2$ (eV) | 0.369 | 0.369 | 0.366 | 0.374 | 0.376 | 0.365 |
| Triplet $H_2O_2$ (eV) | 1.573 | 1.543 | 1.085 | 1.183 | 1.512 | 1.380 |
| Singlet $H_2O_2$ (eV) | 1.400 | 1.229 | 0.760 | 1.044 | 0.527 | -0.414 |
| | 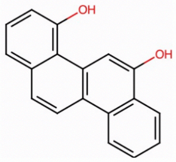 | 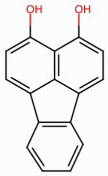 | 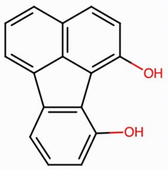 | 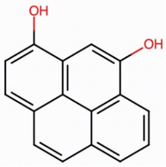 | 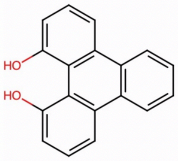 | 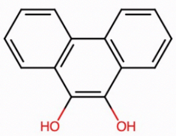 |
| | **Chrysene** | **Fluoranthene (Top)** | **Fluoranthene (Back)** | **Pyrene** | **Triphenylene** | **Phenanthraquinone** |
| Triplet $O_2$ (eV) | 0 | 0 | 0 | 0 | 0 | 0 |
| Singlet $O_2$ (eV) | 0.373 | 0.369 | 0.377 | 0.359 | 0.379 | 0.363 |
| Triplet $H_2O_2$ (eV) | 1.523 | 1.514 | 1.893 | 1.440 | 1.574 | 1.407 |
| Singlet $H_2O_2$ (eV) | 0.865 | 1.686 | 1.305 | 0.319 | 1.241 | 0.013 |

Fig. 3 It is an illustration of the molecules evaluated with the triplet and singlet energies for both the $O_2$ and $H_2O_2$ intermediates. Phenanthraquinone was determined to be the most suitable candidate to explore due to the singlet hydrogen peroxide's energy being the closest to zero. All the rest of the evaluated molecules indicated an endothermic reaction, except for benzo[c]phenanthrene. Benzo[c]phenanthreneone was not chosen as the most suitable candidate because it would be difficult to close the catalytic cycle and reduce it so that it would be able to produce more H2O2.

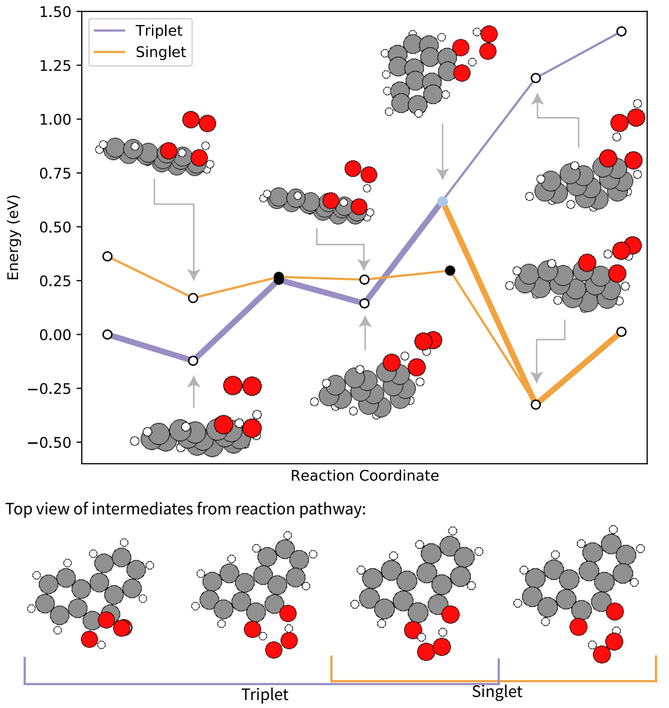

Fig. 4 The triplet and singlet pathways for the conversion of $O_2$ to $H_2O_2$ with phenanthraquinone. The purple line is for the triplet pathway, while the gold line is for the singlet pathway. Black and blue circles represent transition states while white circles represent relaxed intermediates.

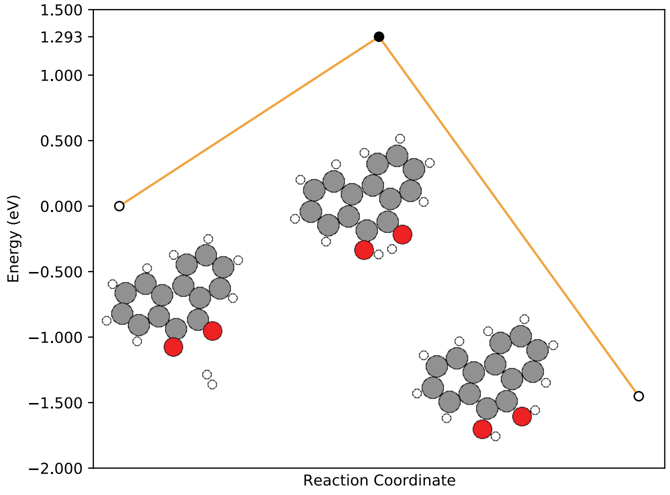

Fig. 5 Reaction pathway for the rehydrogenation of Phenanthraquinone. Black and blue circles represent transition states while white circles represent relaxed intermediates.

tively[30]. The barrier calculated for the regeneration of phenanthraquinone is significantly larger than these values, however, using a Pd catalyst or an alternative reducing agent could dramatically lower this barrier. The removal of Pd from the process would be a positive step since it must be fully extracted after this catalyst regeneration step as it facilitates the breakdown of $H_2O_2$ in the $O_2$ reduction step. An alternative reducing agent might be able to take advantage of simultaneously reducing both oxygen atoms and if that process had a barrier that is comparable to that of the regeneration of AHQ with Pd would dramatically strengthen the case for phenanthraquinone to be an alternative catalyst for $H_2O_2$ production. There are many possible degredation products of AQ that result from this regeneration stage, and these should be studied for phenanthraquinone, especially in the context of different reducing agents, however, this analysis is outside of the scope of this report.

## 4 Conclusion

This paper presents computational results modeling the transition of OOH$^{\cdot}$ across the AHQ molecule and explore alternative catalysts to eliminate the transition. For the AHQ process, it is favorable for the hydroperoxyl to move across the AHQ molecule and fall into a deep well that will slow down the reaction. Based on the previously calculated pathway, the rate determining step was proposed to be too small meaning that $O_2$ dissolution would be the rate limiting factor. This new minima helps to clarify how this is not the case. Alternative molecules which place OH-groups on the same side of similarly sized molecules were explored to determine if a suitable alternative exists where the $O_2$ molecule can be fully reduced in the same location. Multiple molecules were surveyed, and phenanthraquinone was selected for further analysis. The reaction barriers for phenanthraquinone were found to be smaller in comparison to those of the AHQ molecule. Regeneration of phenanthraquinone with $H_2$ had higher barriers than what was previously reported for the reduction of AQ, however, this is without a Pd catalyst that is common to AQ reduction. Being able to reduce phenanthraquinone without the need of a Pd catalyst does present an improvement over the current AQ process since this catalyst must be completely removed so the regenerated catalyst can be used to synthesize $H_2O_2$.

## Conflicts of interest

There are no conflicts to declare.

## Acknowledgements

The authors thank the financial support from the California State University Fullerton as well as computational resources provided by the Center for Computational and Applied Mathematics located at the California State University Fullerton. Additionally, this work used the Extreme Science and Engineering Discovery Environment (XSEDE)[45], which is supported by National Science Foundation grant number ACI-1548562.

## Notes and references

1 N. Sharma, N. K. Bhardwaj and R. B. P. Singh, *J. Cleaner Prod.*, 2020, **256**, 1–11.

2 T. Nishimi, T. Kamachi, K. Kato, T. Kato and K. Yoshizawa, *Eur. J. Org. Chem.*, 2011, **2011**, 4113–4120.

3 R. Ciriminna, L. Albanese, F. Meneguzzo and M. Pagliaro, *ChemSusChem*, 2016, **9**, 3374–3381.

4 X. Tong, W. Shen, X. Chen and J.-P. Corriou, *J. Cleaner Prod.*, 2018, **198**, 1066–1075.

5 F. Lopez, M. Diaz, M. Eugenio, J. Ariza, A. Rodriguez and J. L., *Bioresour. Technol.*, 2003, **87**, 255–261.

6 C. Samanta, *Appl. Catal., A*, 2008, **350**, 133–149.

7 W. Wang, X. Lu, P. Su, Y. Li, J. Cai, Q. Zhang, M. Zhou and O. Arotiba, *Chemosphere*, 2020, **259**, 127423.

8 Y.-f. Zhang, S.-y. Zhang, H. Li, C.-w. Wang, F.-h. Jiang and J.-f. Lyu, *Chemosphere*, 2020, **257**, 127140.

9 J. Teles, I. Hermans, G. Franz and R. Sheldon, *Oxidation*, Wiley, 2015, pp. 11–20.

10 C. Miao, Q. Zhu, Y. Yi, J. Su, N. He, J. Liu and H. Guo, *Ind. Eng. Chem. Res.*, 2019, **58**, 11739–11749.

11 G. Blanco-Brieva, M. Pilar de Frutos-Escrig, H. Martín, J. Campos-Martin and J. Fierro, *Catal. Today*, 2012, **187**, 168–172.

12 S. Fukuzumi, Y. Yamada and K. Karlin, *Electrochim. Acta*, 2012, **82**, 493–511.

13 E. Jung, H. Shin, W. Hooch Antink, Y.-E. Sung and T. Hyeon, *ACS Energy Lett.*, 2020, **5**, 1881–1892.

14 J. S. Jirkovský, I. Panas, E. Ahlberg, M. Halasa, S. Romani and D. J. Schiffrin, *J. Am. Chem. Soc.*, 2011, **133**, 19432–19441.

15 S. Siahrostami, A. Verdaguer-Casadevall, M. Karamad, D. Deiana, P. Malacrida, B. Wickman, M. Escudero-Escribano, E. A. Paoli, R. Frydendal, T. W. Hansen, I. Chorkendorff, I. E. L. Stephens and J. Rossmeisl, *Nat. Mater.*, 2013, **12**, 1137–1143.

16 A. Verdaguer-Casadevall, D. Deiana, M. Karamad, S. Siahrostami, P. Malacrida, T. W. Hansen, J. Rossmeisl, I. Chorkendorff and I. E. L. Stephens, *Nano Lett.*, 2014, **14**, 1603–1608.

17 E. Jung, H. Shin, B.-H. Lee, V. Efremov, S. Lee, H. S. Lee, J. Kim, W. Hooch Antink, S. Park, K.-S. Lee, S.-P. Cho, J. S. Yoo, Y.-E. Sung and T. Hyeon, *Nat. Mater.*, 2020, **19**, 436–442.

18 H. Yang, M. Zhou, W. Yang, G. Ren and L. Ma, *Chemosphere*, 2018, **206**, 439 – 446.

19 H. W. Kim, M. B. Ross, N. Kornienko, L. Zhang, J. Guo, P. Yang and B. D. McCloskey, *Nat. Catal.*, 2018, **1**, 282–290.

20 Z. Lu, G. Chen, S. Siahrostami, Z. Chen, K. Liu, J. Xie, L. Liao, T. Wu, D. Lin, Y. Liu, T. F. Jaramillo, J. K. Nørskov and Y. Cui, *Nat. Catal.*, 2018, **1**, 156–162.

21 C. Xia, S. Back, S. Ringe, K. Jiang, F. Chen, X. Sun, S. Siahrostami, K. Chan and H. Wang, *Nat. Catal.*, 2020, **3**, 125–134.

22 C. Xia, Y. Xia, P. Zhu, L. Fan and H. Wang, *Science*, 2019, **366**, 226–231.

23 P. Landon, P. J. Collier, A. F. Carley, D. Chadwick, A. J. Papworth, A. Burrows, C. J. Kiely and G. J. Hutchings, *Phys. Chem. Chem. Phys.*, 2003, **5**, 1917–1923.

24 J. Zhou, H. Guo, X. Wang, M. Guo, J. Zhao, L. Chen and W. Gong, *Chem. Commun.*, 2005, 1631–1633.

25 Y. Yi, J. Zhou, H. Guo, J. Zhao, J. Su, L. Wang, X. Wang and W. Gong, *Angew. Chem., Int. Ed.*, 2013, **52**, 8446–8449.

26 Y. Yi, J. Zhou, T. Gao, H. Guo, J. Zhou and J. Zhang, *AIChE J.*, 2014, **60**, 415–419.

27 Y. Yi, L. Wang, G. Li and H. Guo, *Catal. Sci. Technol.*, 2016, **6**, 1593–1610.

28 J. M. Campos-Martin, G. Blanco-Brieva and J. L. G. Fierro, *Angew. Chem., Int. Ed.*, 2006, **45**, 6962–6984.

29 G. Goor, J. Glenneberg, S. Jacobi, J. Dadabhoy and E. Candido, in *Hydrogen Peroxide*, American Cancer Society, 2019, pp. 1–40.

30 T. Kamachi, T. Ogata, E. Mori, K. Iura, N. Okuda, M. Nagata and K. Yoshizawa, *J. Phys. Chem. C*, 2015, **119**, 8748–8754.

31 H.-G. Korth and P. Mulder, *The Journal of Organic Chemistry*, 2020, **85**, 2560–2574.

32 J. J. Mortensen, L. B. Hansen and K. W. Jacobsen, *Phys. Rev. B*, 2005, **71**, 035109.

33 J. Enkovaara, C. Rostgaard, J. J. Mortensen, J. Chen, M. Dułak, L. Ferrighi, J. Gavnholt, C. Glinsvad, V. Haikola, H. A. Hansen, H. H. Kristoffersen, M. Kuisma, A. H. Larsen, L. Lehtovaara, M. Ljungberg, O. Lopez-Acevedo, P. G. Moses, J. Ojanen, T. Olsen, V. Petzold, N. A. Romero, J. Stausholm-Møller, M. Strange, G. A. Tritsaris, M. Vanin, M. Walter, B. Hammer, H. Häkkinen, G. K. H. Madsen, R. M. Nieminen, J. K. Nørskov, M. Puska, T. T. Rantala, J. Schiøtz, K. S. Thygesen and K. W. Jacobsen, *J. Phys.: Condens. Matter*, 2010, **22**, 253202.

34 A. H. Larsen, J. J. Mortensen, J. Blomqvist, I. E. Castelli, R. Christensen, M. Dułak, J. Friis, M. N. Groves, B. Hammer, C. Hargus, E. D. Hermes, P. C. Jennings, P. B. Jensen, J. Kermode, J. R. Kitchin, E. L. Kolsbjerg, J. Kubal, K. Kaasbjerg, S. Lysgaard, J. B. Maronsson, T. Maxson, T. Olsen, L. Pastewka, A. Peterson, C. Rostgaard, J. Schiøtz, O. Schütt, M. Strange, K. S. Thygesen, T. Vegge, L. Vilhelmsen, M. Walter, Z. Zeng and K. W. Jacobsen, *J. Phys.: Condens. Matter*, 2017, **29**, 273002.

35 J. P. Perdew, K. Burke and M. Ernzerhof, *Phys. Rev. Lett.*, 1996, **77**, 3865–3868.

36 A. Tkatchenko and M. Scheffler, *Phys. Rev. Lett.*, 2009, **102**, 073005.

37 G. Henkelman, B. P. Uberuaga and H. Jónsson, *J. Chem. Phys.*, 2000, **113**, 9901–9904.

38 E. L. Kolsbjerg, M. N. Groves and B. Hammer, *J. Chem. Phys.*, 2016, **145**, 094107.

39 R. A. Sheldon and J. K. Kochi, *Metal-catalyzed Oxidations of Organic Compounds*, Academic Press, 1981, pp. 17 – 32.

40 L. Valgimigli, R. Amorati, M. G. Fumo, G. A. DiLabio, G. F. Pedulli, K. U. Ingold and D. A. Pratt, *The Journal of Organic Chemistry*, 2008, **73**, 1830–1841.

41 G.-F. Han, F. Li, W. Zou, M. Karamad, J.-P. Jeon, S.-W. Kim, S.-J. Kim, Y. Bu, Z. Fu, Y. Lu, S. Siahrostami and J.-B. Baek, *Nat. Commun.*, 2020, **11**, 2209.

42 D. M. Wang, Y. Zhang, L. L. Zheng, X. X. Yang, Y. Wang and C. Z. Huang, *J. Phys. Chem. C*, 2012, **116**, 21622–21628.

43 D. M. Wang, M. X. Gao, P. F. Gao, H. Yang and C. Z. Huang, *J. Phys. Chem. C*, 2013, **117**, 19219–19225.

44 Y. Wu and S. Han, *J. Lumin.*, 2016, **179**, 595 – 601.

45 J. Towns, T. Cockerill, M. Dahan, I. Foster, K. Gaither, A. Grimshaw, V. Hazlewood, S. Lathrop, D. Lifka, G. D. Peterson, R. Roskies, J. Scott and N. Wilkins-Diehr, *Comput. Sci. Eng.*, 2014, **16**, 62–74.